04,09,16

Electron-hole and exciton processes in CaF_2, SrF_2, and BaF_2 crystals (Review)

© P.A. Rodnyi

Peter the Great Saint-Petersburg Polytechnic University,
St. Petersburg, Russia

E-mail: piotr.rodnyi@gmail.com

Received September 27, 2023
Revised December 13, 2023
Accepted December 14, 2023

The main characteristics of nominally pure CaF_2, SrF_2, and BaF_2 single crystals are presented. Numerous experimental and theoretical data on the crystal and band structures of the compounds under study and their optical properties have been brought together; the analysis and systematization of these data were carried out. It is shown that many features of CaF_2, SrF_2, and BaF_2 are due to their crystal structure. The main parameters of electron (F, M) and hole (V_K, H) point defects are presented, and the mechanisms of their diffusion at low and high temperatures are studied. The transient absorption spectra of defects are explored. The criteria for various channels of defect formation and presumable mechanisms for the decay of self-trapped excitons with the production of point defects and intrinsic luminescence quanta are analyzed. The problem of interpretation of the emission mechanism of singlet excitons is considered.

Keywords: crystals with fluorite structure, point defects, defect formation mechanisms, self-trapped holes and excitons, intrinsic luminescence.

DOI: 10.61011/PSS.2024.02.57911.215

Contents

1. Introduction

Crystals CaF_2, SrF_2 and BaF_2, i. e., alkaline earth fluorides (AEF) with a fluorite structure, are of great interest to researchers. Excellent mechanical, technical and operational characteristics combined with transparency in a wide spectral range, high optical homogeneity and radiation resistance allow the use of single-crystals of calcium fluoride and its analogues in spectrophotometry, photochromic and laser optics, infrared technique, holography, etc. The high degree of ionic coupling of objects leads to special properties of excitons and color centers in them. AEF refer to crystals with an extremely large band gap (> 10 eV), which encourages their use as optical media for the vacuum ultraviolet (VUV) region of the spectrum. An unusual property of the crystals CaF_2, SrF_2 and BaF_2 is that they have a high intensity of intrinsic (exciton) luminescence at room temperature.

In 1950s fluorite crystals with rare-earth impurities were studied in detail by P.P. Feofilov (see for example [1]). Further studies were carried out: in the laboratory of A.A. Kaplyansky, Ioffe Physicotechnical Institute [2]; laboratory of V.V. Osiko, Prolhorov Institute of General Physics [3]; laboratory of A.I. Ryskin, Vavilov State Optical Institute [4]; laboratory of B.P. Sobolev, Institute of Crystallography of RAS [5]; laboratory of V.M. Lisitsyn, Tomsk Polytechnic University [6] etc. The first calculations of the electronic band structure of CaF_2 and its analogues were carried out by N.V. Starostin and employees (at that time using bulky lamp computers) [7]. The synthesis of

crystals CaF_2 by the methods of Stockbarger and Stepanov was developed in the scientific group of V.M. Reiterov (GOI-2) [8]. A great contribution to the preparation and study of fluorite-type crystals was made by the studies of E.A. Radzhabov with employees, Vinogradov Institute of Geochemistry [9].

In the remarkable monograph „Alkaline earth fluorides" edited by W. Hayes [10] the physical processes occurring in AEF were considered, and their main characteristics were given. Since this monograph publication, many changes occurred in the synthesis of AEF-c rystals, methods of their study, and theoretical approaches. A number of new effects for AEF were discovered, in particular, a previously unknown type of radiation BaF_2 — core-valence luminescence [11,12] (see details in p. 4.2). Recently, the use of CaF_2 crystals as materials for microlithography is developed [13]. VUV microlithography requires highly pure samples, and as a result the quality of CaF_2 crystals has been significantly improved [14]. Scintillators based on AEF are known, in particular BaF_2 [12] and $CaF_2:Eu$ [15]. A fluorite crystal with color centers is also a promising holographic medium [4]. Despite the wide range of applications, electron-hole and exciton processes in crystals of the fluorite type remain less studied in comparison with those in the known model objects of condensed matter physics—alkali-halide crystals (AHC).

The above facts indicate the need for a detailed description of the characteristics AEF-crystals, which is done in this paper. Numerous experimental and theoretical data, which do not always correspond to each other, were brought together, and these data were analyzed and systematized. It is shown that many features of CaF_2, SrF_2 and BaF_2 are due to the crystal structure of the objects. MgF_2 crystal is also classified as AEF, but it has a different structure (rutile structure). For short, we denote the objects under study as MeF_2, where Me = Ca, Sr and Ba. Among the crystals MeF_2 the most studied is CaF_2, therefore many characteristics are given for calcium fluoride. However, in a number of cases it is necessary to consider the properties of each of the three crystals separately, taking into account the characteristics of the given object. MeF_2 with rare earth and other impurities (this is a separate and bulk material) will not be described here; the main attention is paid to the so-called intrinsic electron-hole and exciton processes.

2. General characteristics of crystals

2.1. Crystal structure

Crystals MeF_2 have fluorite structure with space symmetry group $Fm\bar{3}m$ (Figure 1) [16,17]. Metal ions (Me^{2+}) in fluorite form a face-centered cubic lattice. Fluorine ions (F^-) have a tetrahedral environment, and each ion Me^{2+} is in the center of a cube of eight equivalent fluorine ions. A feature of the fluorite structure is the alternation of fluorine cubes containing and not containing ion Me^{2+} in the center. The presence of „voids" in cubes of fluorine ions (Figure 1) leads to the fact that the hole component of the autolocalized exciton has configuration that differs from that in AHC (see below). This also promotes the formation of clusters when trivalent rare earth ions (Re^{3+}) [1,3] are introduced into the crystal with fluorite structure. The activator Re^{3+} replaces the cation Me^{2+}, and the excess charge of the activator is neutralized by ion F^- located in „empty" fluorine cube, i. e. in the form of an interstitial ion (charged interstitial). With increase in the cation radius $r(Me^{2+})$ the lattice constant a increases (Table 1), and it turns out that in BaF_2 ions fill only 52% of space (in the approximation of hard spheres).

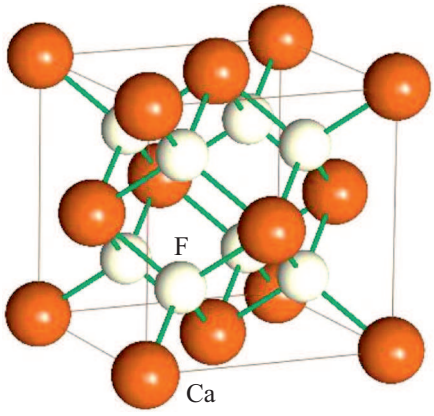

Figure 1. Fragment of crystal structure CaF_2.

Table 1. Parameters of fluorite-type crystals [18,19]: a — crystal lattice constant; $r(F^- - F^-)$ — distance between fluorine ions; $r(Me^{2+})$ — ionic radius of the cation for coordination number 8 (ionic radius of fluorine $r(F^-) = 1.15$ Å); I — degree of ionic coupling; ε_s and ε_∞ — stationary and high-frequencydielectric permittivity, respectively; $\hbar\omega_{LO}$ — optical phonon energy

MeF_2	a, Å	$r(F^- - F^-)$, Å	$r(Me^{2+})$, Å	I, %	ε_s	ε_∞	$\hbar\omega_{LO}$, meV
CaF_2	5.46	2.73	1.26	85	6.63	2.04	58
SrF_2	5.78	2.90	1.39	85	6.20	2.07	47
BaF_2	6.17	3.09	1.56	86	6.04	2.15	42

2.2. Band structure

The energy band structure of crystals MeF_2 was determined by measuring spectra: reflection [20,21], characteristic electron losses [21,22], dielectric permittivity [21] and excitation of intrinsic luminescence [23]. A critical analysis of the results obtained, which do not always correspond to each other, was carried out in [24].

Excitation spectrum of intrinsic (exciton) luminescence CaF_2 is shown in Figure 2 [23]. Here „primary" anion exciton (E_{ex}^a) with an energy of 11.18 eV is designated as E_1. At energies exceeding E_1, a number of exciton maxima

Table 2. E_g — the value of the crystal band gap for direct ($\Gamma \to \Gamma$) and indirect ($X \to \Gamma$) transitions; E^a_{ex} and E^c_{ex} — position of maxima of „primary" anion and cation (core) excitons, respectively [20,21]; ΔE_v — valence band width [34]. Data for room temperature, all values are in eV

Crystal	E_g, $\Gamma \to \Gamma$	E_g, $X \to \Gamma$	E^a_{ex}	E^c_{ex}	ΔE_v
CaF_2	12.1	11.80	11.2	25.0	3.10
SrF_2	11.25	10.60	10.7	22.4	2.80
BaF_2	11.0	10.0	10.2	17.2	2.50

is recorded, they are determined by transitions from the valence band to higher levels of the conduction band.

The energy $(E_g + E_1) = 23.3$ eV, where E_g — the band gap, corresponds to the beginning of photon multiplication, at which the incident photon creates two electron-hole pairs (steep rise of the curve in Figure 2 at $E > 23.3$ eV). Note that the mechanism of photon multiplication was first discovered and interpreted at the AHC by Ch.B. Lushchik and employees [25]. The „primary" cation (or core, $3p$Ca) exciton (E_c) is formed at energies slightly exceeding 25 eV. This is followed by maxima at 29.2, 30.6, 32.8 and 34.4 eV, which are attributed to the transitions of $3p \to 3d$ and $3p \to 4s$ ion Ca^{2+} [20.23].

Using especially pure CaF_2, it was possible to study Urbach tails at the absorption blue edge of the crystal [26]. It was shown that the temperature-dependent part of the absorption edge is due to the interaction of excitons with optical phonons, and the temperature-independent part is due to residual impurities in the crystal [26,27].

The first calculations of the band structure of CaF_2 and its analogues were carried out in the 1970s by methods of strong coupling, linear combination of atomic orbitals and added plane waves; analysis of such data was carried out in paper [28]. Further, calculations of the band gap MeF_2 were carried out using the Hartree–Fock (HF) method [29,30] and density functional theory (DFT) [16,31]. In the first case the results were overestimated, and in the second, underestimated values E_g, so researchers began to use complex calculation methods [32,33]. Figure 3 shows a diagram of the energy bands CaF_2 [32]. The filled valence band is formed predominantly by orbitals $2pF^-$; the states $3pCa^{2+}$ are responsible for the upper core band; the bottom of the conduction band is formed by the states $3d$ and $4s$ of the ion Ca^{2+}.

Table 2 shows the main parameters of the band structure of crystals MeF_2 obtained on the basis of experimental [20,21] and theoretical [32] data.

The value E_g is determined by transitions from the valence band to the conduction band in the center of the Brillouin zone; the values of indirect ($X \to \Gamma$) transitions are also given. The position and width (ΔE_v) of the valence band were determined from photoelectron spectroscopy data [34,35].

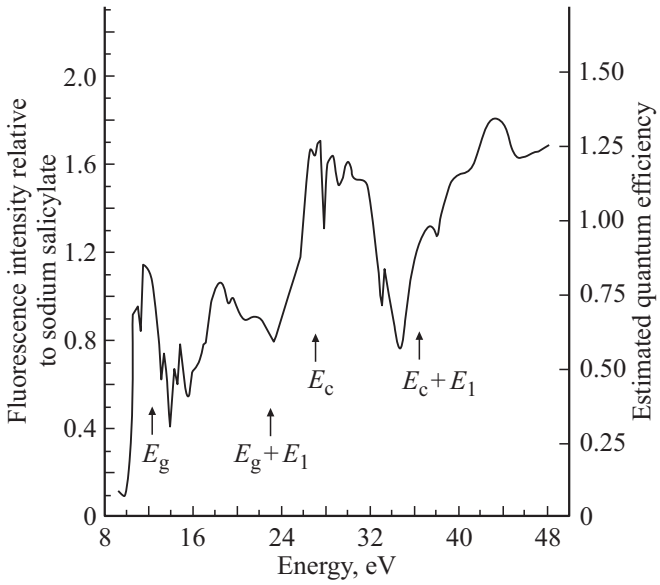

Figure 2. Excitation spectrum of intrinsic (exciton) luminescence CaF_2at 77 K [23].

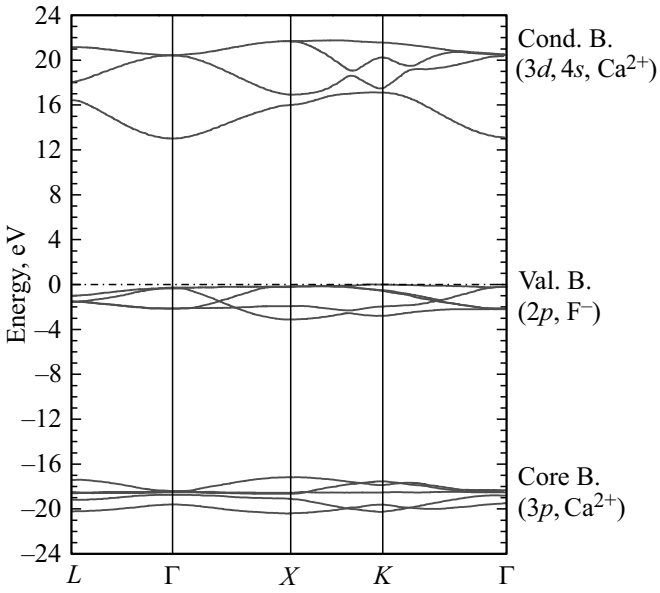

Figure 3. Band structure elements CaF_2 relative to the Fermi level (dashed-dot line) [32].

The use of two-tone excitation with excimer laser made it possible to identify the exciton peaks at the fundamental absorption edge of the crystals CaF_2 and BaF_2 [36]. The following band gap values were obtained CaF_2: 12.0 ± 0.1 and 11.8 ± 0.1 eV at 15 and 298 K, respectively, and BaF_2: 10.6 ± 0.1 eV at 298 K.

2.3. Optical characteristics

Table 3 shows the main characteristics of fluorides used as windows, prisms and lens in wide spectral range: from

Table 3. Main characteristics of fluorides used as optical materials: $\lambda_{min}-\lambda_{max}$ — transparency range; n — refraction index for wavelength 157 nm [37]; D — density; molecular weight; solubility in 100 g of water at 20°C; T_{melt} — melting point

Crystal	$\lambda_{min}-\lambda_{max}$, μm	n	D, g/cm^3	Mol. weight	Solubility, g/100g H_2O	T_{melt}, °C
CaF_2	0.13–10	1.559	3.18	78.08	0.0017	1360
SrF_2	0.15–11	1.575	4.24	125.6	0.012	1450
BaF_2	0.20–12	1.656	4.88	175.36	0.17	1368
MgF_2	0.12–7	1.476	318	62.32	0.0002	1255
LiF	0.12–6	1.485	2.639	25.94	0.27	848

VUV to IR. LiF and MgF_2 have the absorption blue edge, so they are used when working with the hydrogen line 121 nm. For BaF_2 the IR range is the priority.

Among the fluorides presented, CaF_2 has the best characteristics: high transparency in the VUV region of the spectrum, resistance to laser radiation, low axial and radial birefringence, uniformity of the refractiion index, lack of hygroscopicity. These characteristics make CaF_2 a convenient material for microlithography using excimer lasers emitting at 193 and ~ 157 nm [13]. Note that CaF_2 crystals of UV-class require a higher level of purity compared to IR-class crystals, which necessitates special technological methods when synthesizing samples [37].

3. Point defects (color centers)

3.1. Preliminary remarks

During interband (valence band — conduction band) excitation in ionic crystals the autolocalized holes or V_K-centers are formed [38,39]. For AHC the model of V_K-center in the form of a molecular ion X_2^- was established by methods of EPR [40] and electron-nuclear double resonance (ENDR) [41]. The distance between the haloid ions in V_K-center in AHC turned out to be by 30–40% less than that in an ideal lattice. Theoretically, the process of formation of the two-haloid ion of the molecular ion X_2^- was studied in [38,39,42]. It is shown that due to the Yang-Teller effect an additional gain in energy appears during hole autolocalization, and non-fully symmetric vibrations lead to hole localization on two neighboring haloid ions.

V_K-center can capture the electron from the conduction band and form the autolocalized exciton (ALE) in the form $e^0(V_K + e)$. In AHC series the molecular ion X_2^- is displaced along its axis, and the remaining anion vacancy captures the electron. As a result, instead of the usual ALE in the form $(V_K + e)$ with symmetry D_{2h} (on-center) a state is formed similar to a pair of nearby F^- and H-centers (off-center, symmetry C_{2v}) [43]. ALE characteristics in MeF_2 are discussed in [44].

Under the influence of ionizing radiation in AHC, in addition to V_K-centers, the Frenkel pairs F–H and other point defects (color centers) are formed [45,46]. In some cases a pair of anion vacancy (α-center) and interstitial anion ion (I-center) is formed. Frenkel pairs of defects (F–H and α–I) in AHC can be effectively created not only during high-energy excitation of the crystal, but also in the region of exciton formation — exciton mechanism of defect formation (see more details in [46]).

3.2. Basic parameters of defects

The results of early (before 1974) studies of point defects in crystals MeF_2 are presented in detail in [10] (Chap. 4). The fluorides under consideration turned out to be more resistant to irradiation compared to AHC. At room temperature the nominally pure CaF_2 crystals are not colored when exposed to X-rays. Even at low temperatures ($T \leq 77$ K) the efficiency of color center formation is low, especially in CaF_2. To create point defects in MeF_2 hard radiation (neutrons, high-energy electrons, gamma rays) is required. Residual impurities may participate in the process of defect formation; for this reason, the experimental data obtained on the optical properties of color centers in crystals do not always correspond to each other. Color centers in MeF_2 were studied by EPR and ENDR methods, as well as by measuring magnetic circular dichroism [10]. Sometimes, in order to study a specific defect (in particular, V_K-center), an impurity of a rare earth ion is introduced into the crystal. Defects are created predominantly in the anion sublattice due to differences in the formation energies of anion and cation Frenkel pairs; for example, in CaF_2 the corresponding energies are 2.75 and 8.0 eV [30].

Electronic (F, M) and hole (V_K, H) color centers in MeF_2 are characterized by absorption bands in the visible and near UV regions of the spectrum (Table 4).

The width (half-width at half-maximum $\Delta E_{1/2}$) of the absorption bands V_K- and H-centers is ~ 1 eV, while the maxima of the bands are quite close.

As a result, the absorption bands of V_K-centers in MeF_2 were identified using polarization methods [47]. Next, we will consider the characteristics of each of the color centers separately. Attention will be paid to centers created by VUV or X-ray quanta, since irradiation with heavy particles leads to the appearance of additional defects in the crystal.

Table 4. Maxima of absorption bands (in nm) of electronic (F, M) and hole (V_K, H) color centers in MeF_2at $T \leq 77$ K according to [10,47]

Crystal	F	M	V_K	H
CaF_2	376	521	320/~750	308
SrF_2	433	595	326/~750	308
BaF_2	611	–	336/~750	330

3.2.1. α-centre. An anion vacancy (α-center) is formed when the fluorine ion is displaced from a regular position into interstice of a cube of eight fluorine ions (I-center); or it exists in MeF_2 in the form of a compensating charge if the crystal contains monovalent alkali metal ions. The creation of α-center precedes the formation of F-center, the calculated energy value for the creation of anion vacancy in CaF_2 is: 7.87 eV [10], as per other data, 8.34 eV [48]. The theoretical value of the diffusion energy of α-center is 0.33, 2.67 and 2.74 eV for the directions $\langle 100\rangle$, $\langle 110\rangle$ and $\langle 111\rangle$ respectively [48]. Consequently, the preferred direction of the anion vacancies migration is $\langle 100\rangle$, which is consistent with experimental data [48].

3.2.2. F-centre. In the structure of fluorite, the F-center (a fluorinevacancy that captured the electron) is located in the center of a tetrahedron of four ions Me^{2+} (insert in Figure 4). Point symmetry group of the center — T_d (in AHC — O_h). In the second coordination sphere six fluorine ions are located at the corners of the octahedron. According to calculations [49], in CaF_2 ions Ca^{2+} are displaced from the F-center by ~ 0.09 Å, and the displacement of the nearest ions F^- towards the center is 0.14 Å. The maximum of the absorption band of F-center in CaF_2 is at 3.3 eV (376 nm), and the main level of the center is located by 1.5−2.0 eV below the bottom of the conduction band [30]. For BaF_2, the maximum of the absorption band and the depth of the F-center are 2.03 and 1.7 eV, respectively [49]. Ionization of F-centers upon illumination into the corresponding absorption band was used to measure the Hall mobility of electrons, which in MeF_2 turned out to be low: $\sim 50\,cm^2/(V\cdot s)$at 200 K [50]. The released electrons, when illuminated into F-absorption band, can be captured by V_K-centers and form exciton states [51].

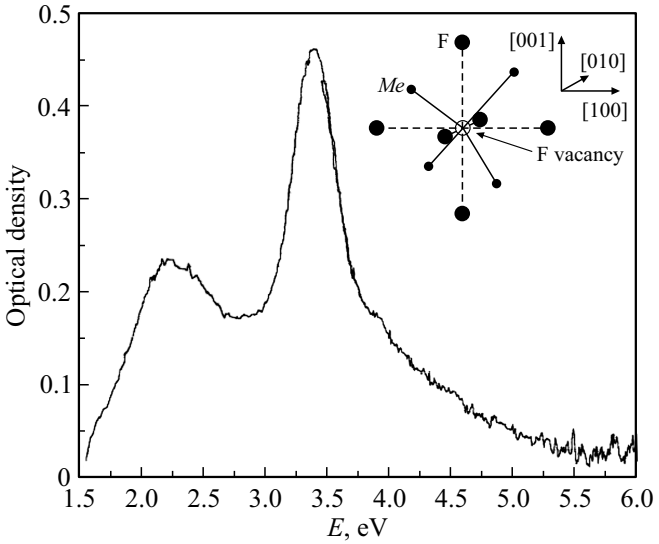

Figure 4. Steady-state absorption spectrum of nominally pure crystal BaF_2 irradiated with X-ray (40 kV, 50 mA) quanta for 30 min at 80 K [52]. Insert: configuration of F-center in the fluorite structure.

Figure 4 shows the absorption spectrum of nominally pure crystal BaF_2 irradiated with X-ray (40 kV, 50 mA) quanta for 30 min at 77 K (CaF_2 not colored under such conditions) [52]. The spectrum is characterized by two broad bands with maxima at 2.3 eV (540 nm) and 3.4 eV (365 nm), for which F- and V_K-centers (EPR data), respectively. The displacement of the band maxima compared to those given in Table 4 is explained by the fact that in earlier studies were carried out on BaF_2 crystals with a thulium impurity [47].

F-centers (and more complex electron centers) in CaF_2 can be created at room temperature by irradiation with high-energy electrons [53,54], gamma quanta [ ]55} and neutrons [56]. During electron (280 keV) irradiation of a nominally pure CaF_2 crystal the absorption bands with maxima 2.70, 2.91, 3.09, 3.30 eV, belonging to F-centers, and 3.825, 4.03, 4.30, 4.83 eV, attributed by the authors to H-centers [54] were registered. Under gamma irradiation CaF_2 (1.25 MeV), in addition to the known absorption band 380 nm (F-centers), bands 349, 409 and 478 nm were recorded, the hole color centers are responsible for them [55].

3.2.3. M-, R- and other complex centers. M-center is a formation of two neighboring anion vacancies that captured two electrons (otherwise, two neighboring F-center or F_2-center). In the fluorite structure M-centers can be oriented along $\langle 100\rangle$ or $\langle 110\rangle$ axes. The absorption spectra of the centers are characterized by long-wavelength (transitions $^1\Sigma_g \rightarrow {}^1\Sigma_u$) and short-wavelength (transitions $^1\Sigma_g \rightarrow {}^1\Pi_u$) bands; the latter are located in the absorption region of F-centers [57]. In contrast to F-centers, whose luminescence is not observed in MeF_2, M-centers luminesce intensely when excited in both absorption bands.

The efficiency of formation of M-centers (as well as F-centers) in MeF_2 crystals at room temperature is extremely low. The introduction into crystals of monovalent cationic impurities (Na^+, K^+, Li^+) allows one to obtain M_A-centers (M-centers near the impurity) [58]. These centers are thermally stable — remain stable up to 340−370 K. The luminescence bands of M_A-centers have high intensity, large half-width ($\Delta E_{1/2}$) and short decay time (τ). For example, in CaF_2 : Na the luminescence band has the following characteristics: maximum of the emission band is $\lambda_m = 762$ nm; $\Delta E_{1/2} \approx 0.5$ eV; $\tau = 23$ ns. Such characteristics made it possible to obtain the generation of induced emission of M_A-centers in CaF_2 : Na and SrF_2 : Na crystals at room temperature [59].

Three adjacent F-centers form an R-center (or F_3-center). Larger clusters of F-centers represent a region in the crystal free of fluorine. Diffusion of F-centers can lead to the formation of metal colloids [60] and nanocrystals [61]. This process is especially effective in CaF_2, since the crystal lattice constants of fluorite (Table 1) and metallic calcium ($a = 5.58$ Å [60]) are close. Note that associates/aggregates of F-type centers (F_n) and the process of metal colloids formation in CaF_2 and other ionic crystals were studied in detail in [62].

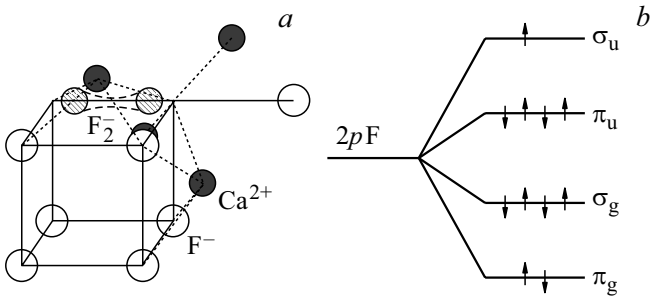

Figure 5. *a*) Model of the molecule F_2^- (V_K-center) in the fluorite structure; *b*) qualitative scheme for the formation of energy levels of molecule F_2^-.

3.2.4. V_K-centre. Autolocalized hole (V_K-center) in MeF_2 is a dumbbell-like molecular ion F_2^-, occupying two anion sites with the internuclear axis oriented along the direction $\langle 100\rangle$ (Figure 5). With the exception of the direction, the properties of V_K-center in crystals with fluorite structure are similar to those in AHC with the symmetry of the centers D_{2h}. The right side of Figure 5 shows a simplified (not considering the crystal field) diagram of the energy levels of molecular orbitals arising from $2p$-states of fluorine [63]. The molecular ion F_2^- contains $11p$-electrons, which in the ground state are located in bonding (σ_g and π_u) and antibonding (π_g and σ_u) orbitals. The ground state of system —

$$\sigma_g^2\pi_u^4\pi_g^4\sigma_u(^2\Sigma_u).$$

The excited states, in order of increasing energy, are as follows:

$$\sigma_g^2\pi_u^4\pi_g^3\sigma_u^2(^2\Pi_g),\quad \sigma_g^2\pi_u^3\pi_g^4\sigma_u^2(^2\Pi_u),\quad \sigma_g\pi_u^4\pi_g^4\sigma_u^2(^2\Sigma_g).$$

Allowed electric dipole transitions $^2\Sigma_u \rightarrow {}^2\Sigma_g$ with vector **E**parallel to the molecular axis (σ-type) are responsible for intensive UV absorption bands of V_K-centers in MeF_2 (Table 4). Long-wave absorption (~ 750 nm) corresponds to $^2\Sigma_u \rightarrow {}^2\Pi_g$ transitions with predominant π-polarization (perpendicular to the axis). Note that for the first time the absorption band of V_K-centers in CaF_2 with maximum 320 nm was identified in paper [64].

According to EPR data, the distance between two haloids in V_K-center CaF_2 is 1.85 Å, and it varies little in the series of crystals CaF_2, SrF_2 and BaF_2 [10]. The theoretical value of this distance varies from 1.84 to 1.96 Å, depending on the calculation model [65]. In any case, the distance between the hal0ids in V_K-center CaF_2 is less than that in the regular lattice (Table 1), which indicates a significant axial relaxation of the ion F_2^-. According to EPR data, the positive charge of the hole is concentrated predominantly at V_K-center; only 2% of the state belongs to neighboring fluorine ions located along $\langle 100\rangle$ axis [47]. The level position of V_K-center relative to the top of the valence band, determined by the molecular dynamics method, is 1.2, 1.4 and 1.6 eV for CaF_2, SrF_2 and BaF_2respectively [66].

3.2.5. H-centre. H-center in MeF_2 is interstitial fluorine atom, covalently bonded to a fluorine ion located at a regular site. According to EPR data [67], the bond runs along $\langle 111\rangle$ axis of the crystal; as a result, H-center, as well as V_K-center, is a diatomic molecular ion of haloid F_2^- with system of energy levels similar to that shown in Figure 5. The unpaired electron at the quasi-molecular σ_u-level of the H-center provides the presence of EPR signal. As a result, H- and V_K-centers are easily distinguishable in the EPR spectra [28], which is difficult in the case of absorption spectra. In contrast to V_K-center, in H-center the electric charge is not uniformly distributed: about 65% of the hole is concentrated on the interstitial fluorine, and about 35% on the fluorine located near a regular site [68]. The distance between the H-center nuclei is 1.90, 1.922 and 1.912 Å in CaF_2, SrF_2 and BaF_2, respectively [69], which is significantly less than the distances between fluorine ions in regular lattice (Table 1).

In [70] the stability of H-centers oriented along $\langle 100\rangle$ and $\langle 111\rangle$ axes in CaF_2 is theoretically reviewed, and It is shown that from energy considerations H$\langle 111\rangle$-configuration is more stable. The distortion of the crystal lattice in the immediate environment of the Hcenter turned out to be greater than in the case of the F-center [71]. The ground level of the H-center is located by 2.97 and 2.93 eV above the top of the valence band in CaF_2 and BaF_2, respectively [68].

3.2.6. I-centre. The I-center is fluorine ion located in the center of the „empty“ fluorine cube MeF_2. Since the shell of the interstitial fluorine ion, F_i^-, or I-center is filled, it weakly interacts with neighboring ions at regular lattice sites. The I-center in MeF_2 does not manifest itself either in EPR experiments or in optical absorption spectra, for this reason the I-center is poorly studied. By recombination with the V_K-center the I-center is transformed into H-center. In some cases, there is a distortion of the absorption band of F-centers under the influence of nearby I-centers [47]. I-centers are effectively created in crystals activated by trivalent rare earth ions. Recently, when studying the core-valence luminescence of crystals $BaF_2:Y^{3+}$ and $BaF_2:Yb^{3+}$, it was possible to show that the ground level of the I-center in BaF_2 is located in the band gap by ~ 0.6 eV above the top of the valence band [47]. Note also that interstitial fluorine ions or I-centers play an important role in the high-temperature ionic conductivity of MeF_2 crystals (see p. 4.2.2).

3.2.7. Autolocalized exciton. Excitons in ionic crystals exist in the form of free and immobile; the latter can be localized on one or two haloids [38,46]. The two-haloid ALEs in MeF_2 are of greatest interest. A non-equilibrium hole created in the crystal by high-energy excitation is thermalized during $10^{-11}-10^{-12}$ s and then, as a result of axial relaxation (during $\sim 10^{-11}$ s) forms V_K-center (Figure 6, *b*) [69]. V_K-center captures the electron from the conduction band, which leads to the formation of exciton of $e^0(V_K + e)$ type. It turned out that in MeF_2 this exciton state (on-center) turns out to be unstable, and

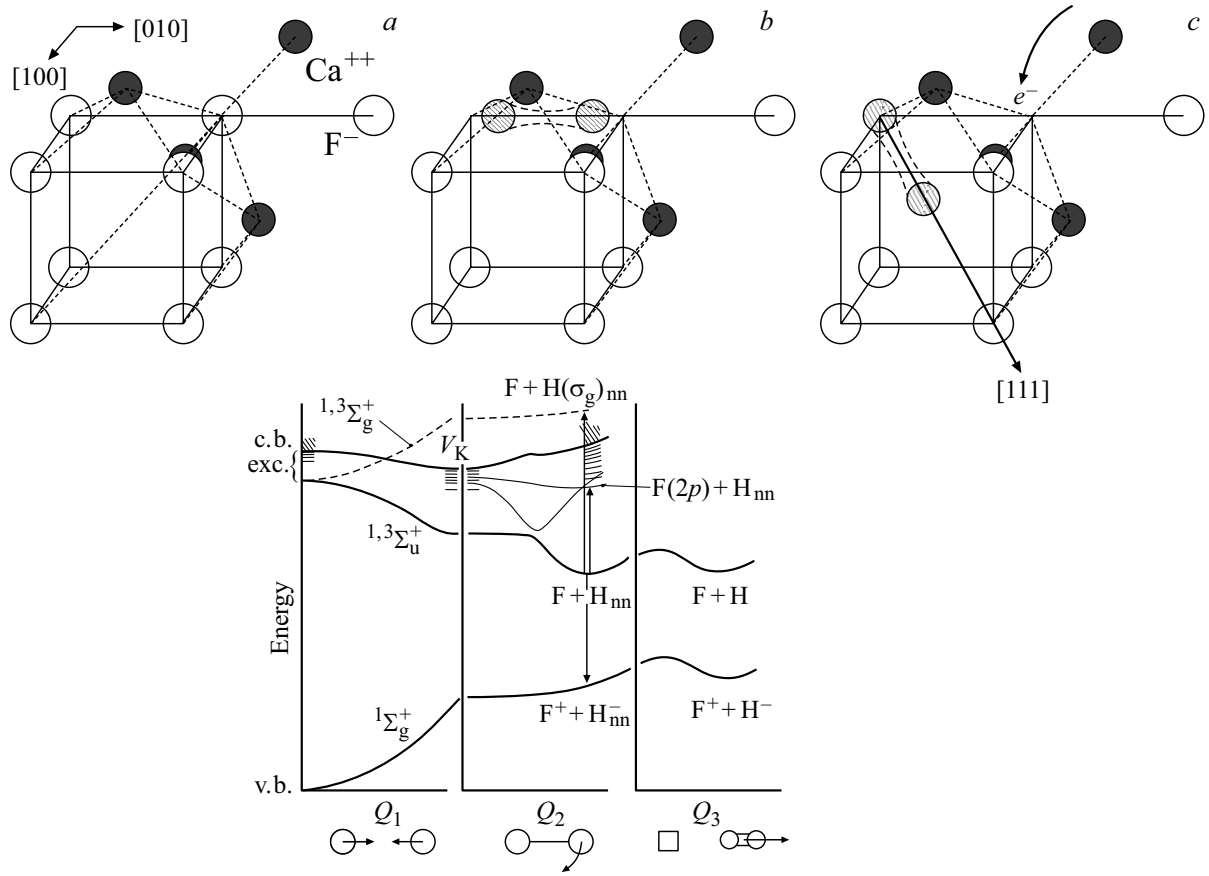

Figure 6. *a*) Fragment of regular crystal structure CaF_2; *b*) autolocalized hole (V_K-center); *c*) autolocalized exciton having the configuration of a pair of nearby F−H centers. Below — energy diagram displaying the phases of exciton relaxation: approach of fluorine ions (Q_1), rotation of the axis of the two-haloid molecule (Q_2), separation of F−H-pair (Q_3) [72].

when the electron is captured, the axis of the two-haloid ion rotates F_2^- (V_K-center) from the direction $\langle 100 \rangle$ to the direction $\langle 111 \rangle$ (Figure 6, *c*). In this case, the electron is captured by the released vacancy, and the hole is localized on the molecular ion F_2^-, forming the H-center. Thus, in crystals with fluorite structure the hole, as an integral part of the ALE, is located on the molecular ion F_2^- oriented in the direction $\langle 111 \rangle$, and the electron is located on the neighboring F-center. ALE configuration as a pair F−H (off-center) in MeF_2 (Figure 6, *c*) differs significantly from that in AHC (p. 3.1).

ALE configuration of in MeF_2 in the form of pair of nearby F−H-centers was established by optical detection of magnetic resonance (ODMR) [73,74]. In [70] CaF_2 crystal was irradiated at temperature of 1.2 K in a resonant cavity with X-ray flux creating ALE, the radiation of which was used to detect the ODMR signal. In [74] CaF_2 crystal was subjected to X-ray irradiation at 77 K to create V_K- and F-centers in it. Then the sample was placed into the resonant cavity, the ODMR spectrum was recorded at temperature of 2 K by illumination into F absorption band. In both cases [73,74] it was reliably shown that the ALE in MeF_2 is a pair of nearby F−H-centers (Figure 6, *c*).

F−H-model of ALE in MeF_2 was also confirmed in experiments on measuring the spectra of the so-called transient absorption [53,75]. The sample was irradiated with short (5 ns) high-energy (500 keV) electron pulses, which create a significant number of ALE in the crystal [75]. The long lifetime of ALEs (tens of microseconds at helium temperatures) allows them to be transferred to higher excited states under the influence of a light beam (xenon lamp or laser). It turned out that the transient optical absorption spectra of MeF_2 crystals subjected to electron irradiation at 10 K contain two main bands (for CaF_2 the spectra are given in Figure 7).

A broad UV absorption band (with maxima at 4.2, 4.1 and 4.0 eV in CaF_2, SrF_2 and BaF_2 respectively) is responsible for the excitation of ALE hole component (H-center) and corresponds to the hole transition from the antibonding orbital σ_u to the bonding orbital σ_g (see diagram in Figure 5). Low-energy bands (with maxima at 2.9, 2.5 and 1.8 eV in CaF_2, SrF_2 and BaF_2, respectively) reflect the excitation of ALE electronic component (transitions $1s \rightarrow 2p$), they are similar to the corresponding absorption of F-centers [75]. Thus, in transient absorption experiments it is possible to excite separately the electron and hole components of ALE.

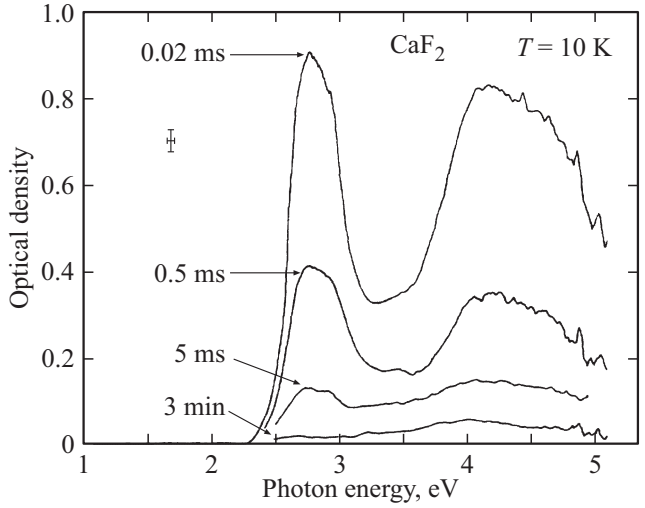

Figure 7. Transient absorption spectra of the crystal CaF_2 after excitation by pulsed flow of high-energy (500 keV) electrons (the delay time after the end of the excitation pulse is indicated) [75].

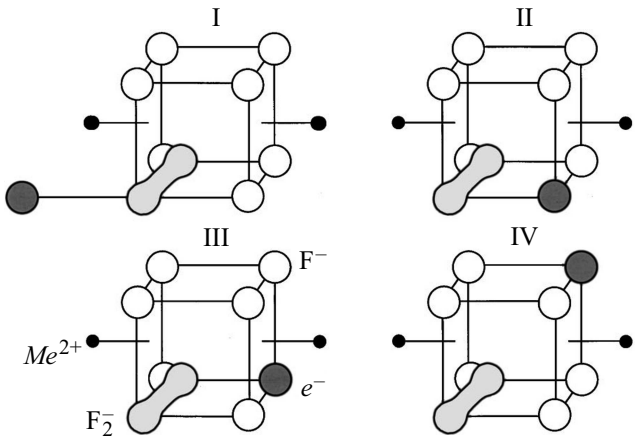

Figure 8. Possible configurations of autolocalized exciton in MeF_2 in the form of nearby H-center (dumbbell-like ion F_2^-) and F-center (dark circles).

The papers [75–78] discussed four possible ALE configurations in the form of pair F−H in crystals with fluorite structure (Figure 8). With respect to the H-center, the neighboring F-center can be located as follows: I — along the edge of the cube, but in the adjacent cell; II — along the edge of the cube in the same cell; III — along the diagonal of the cube plane; IV — along the diagonal of the cube. ALE shown in Figure 6, *c* corresponds to the configuration II of Figure 8. There are some experiment confirmations of such four configurations presence in MeF_2. In SrF_2 it was possible to separate the components of transient absorption by the decay time [79]. The fast component (59 μs) has two pronounced absorption bands at 2.34 (F) and 4.13 eV (H), belonging to the configuration $(F-H)_{II}$. The slow component (7.7 ms) with absorption bands of 2.85 and 3.35 eV is attributed by the authors to the configuration $(F-H)_{III}$. The authors [54] identified in CaF_2 transition absorption bands of all four ALE configurations and studied their interconversion.

Theoretical results of review of possible ALE configurations in MeF_2 are in some contradiction with each other. In [77,78] preference is given to the configuration $(F-H)_{II}$. Calculations [79] showed that the energy characteristics of the formation of ALE off-center are approximately the same for configurations I, II, III (configuration IV was not considered due to the large distance between F- and H-centers). It is noted that to obtain the configuration $(F-H)_{III}$ from the starting $(V_K + e)$ system, the molecular ion F_2^- shall undergo the process of bond switching. According to data [80], the configuration $(F-H)_{III}$ does not exist (there is no minimum of the potential curve), and the most stable configuration $(F-H)_{II}$ is.

3.3. Defect diffusion

3.3.1. Low temperature region. As noted, stable point defects in MeF_2 are effectively formed under the influence of ionizing radiation only at low ($T \leq 77$ K) temperatures [10]. In contrast to AHCs, in which the primary defects are pairs F−H (less often α−I), in MeF_2 the defect complementary to the F-center is the VK center, supplemented by interstitial fluorine ion (I-center). F-centers remain stable (immobile) up to room temperatures, and V_K-centers, starting from certain temperatures, can diffuse throughout the crystal.

Figure 9 shows the temperature dependence of the concentration of hole centers (EPR data) in SrF_2 : Tm crystal irradiated at 77 K. Similar dependences were also obtained for calcium and barium fluorides [81]. X-ray irradiation creates in the crystal V_K-centers (H-centers are practically absent), which become mobile at temperatures exceeding 110 K. Mobile V_K-centers (autolocalized holes) interact with I-centers, which at $T \geq 120$ K are transformed into

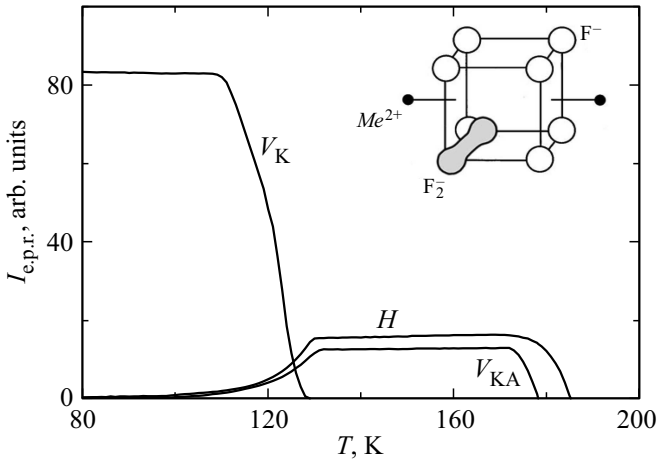

Figure 9. Temperature dependence of the concentration of hole (V_K, H, V_{KA}) centers in the crystal SrF_2 : Tm [83]. Insert: model of the H-center in crystals with fluorite structure.

H-centers by the reaction $(V_K + I) \rightarrow H$. Some V_K-centers interact with impurities, forming V_{KA}-centers (Figure 6). At $T > 200$ K the EPR signal of hole centers was not detected, but it is assumed that they can exist in the crystal in the form of non-paramagnetic centers [75].

It is known that the movement of V_K-centers in MeF_2 crystals occurs by hopping diffusion, i. e., in the form of a sequence of random independent hops between equivalent sites in the lattice [75]. The system of fluorine ions in fluorite crystals is a simple cubic lattice in which two types of movement are possible for the V_K-center: movement along the axis (hops 0 or 180°) and rotation of the axis ofcenter by 90°. The autolocalized hole (V_K-center), which has a strong bond with phonons, is a typical small-radius polaron, which made it possible to calculate the activation energy 180°- and 90°-hopping diffusion of V_K-centers in MeF_2 [82]. The calculated values of activation energy are in satisfactory agreement with experiment. It was shown that CaF_2 is characterized by diffusion along the axis V_K-center (180°-hops), and for SrF_2 and BaF_2 at certain temperatures — reorientation (90°-hops). The obtained diffusion parameters of V_K-centers in MeF_2 crystals are given in Table 5.

For the diffusion activation energy of H-centers in the temperature range 170–200 K, values of 0.40, 0.51 and 0.60 eV were found for CaF_2, SrF_2 and BaF_2 respectively [66].

Subsequently, the molecular dynamics method was used to obtain activation energy values closer to the experimental ones (Table 5) [66]. In addition, the process modeling showed that in BaF_2 and SrF_2 crystals, during the diffusion of the V_K-center a so-called intermediate state arises. This state is realized as a result of the exit of one of the fluorine ions forming the V_K-center into the nearest interstitial site while maintaining the bond with the second fluorine ion of the center. The intermediate state can be considered as a pair of H-center and the nearest anion vacancy. As a result, in crystals BaF_2 and SrF_2 there is an additional diffusion channel of V_K-center through intermediate state, which is not a stable configuration of autolocalized hole and exists for a short period of time [66].

Table 5. Parameters that determine the hopping diffusion of V_K-centers in crystals MeF_2: delocalization temperature T_D, direction of center axis reorientation, activation energy E_a

Parameter	CaF_2		SrF_2		BaF_2	
T_D, K [10,47]	90	120	110	120	95	115
Reorientation, deg [47]	180	180	180	90; 180	90; 180	90; 180
E_a, eV (exp.) [81]	0.19	0.31	0.21	0.30	0.30	0.38
E_a, eV (theor.) [66]	0.20	0.33	0.25	0.36	0.36	0.41
E_a, eV (theor.) [66], Intermediate state	–	–	–	0.4	–	0.28

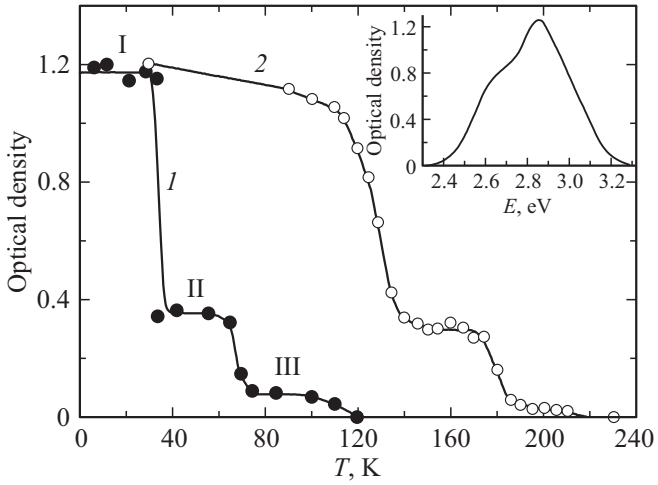

Figure 10. Temperature dependence of the accumulation efficiency (curve *1*) and thermal stability (curve *2*) of F-centers in SrF_2. Insert: spectrum of the F absorption band in SrF_2 crystal irradiated with X-ray flux at 32 K [85].

Note that the delocalization of hole color centers is also effectively manifested in thermally stimulated luminescence (TSL) curves. The spectral composition of TSL crystals irradiated with X-ray quanta [51,83] or neutrons [84] shows that in low-temperature thermopeaks (110–130 and 134–152 K) Ale radiation appears, and in high-temperature (170–300 K) — longer wavelength radiation is caused by the recombination interaction of distant centers. The activation energies for the hole centers movement found from the TSL curves are in accordance with those determined from the EPR data (Table 5).

Concentration of F-centers vs. absorbed dose has two well distinguishable stages: 1) initial, in which F-centers associated with I-centers are formed, as well as V_K-centers; 2) relatively slow second stage, which is characterized by the creation of isolated F- and I-centers [84]. The second stage quickly saturates at concentrations of F-centers $\sim 2 \cdot 10^{18}$ cm^{-3}. This stage cannot be associated with the presence in MeF_2 of initial vacancies, the concentration of which is low.

Let us consider the temperature dependences of the accumulation of F-centers using the example of SrF_2 (curve *1*, Figure 10). The crystal was subjected to X-ray (50 kV, 40 mA) irradiation for an hour, the concentration of F-centers at given temperature was estimated from the value of the absorption spectrum (insert in Figure 10). As can be seen, the dependence of the efficiency of accumulation of F-centers on temperature has a stepwise nature, noticeable drops were recorded at 34 and 67 K (curve *1*, Figure 10). Then, in the region of delocalization of V_K-centers (110 K), the efficiency of accumulation of F-centers decreased to very small values. The temperature regions 4–34, 34–67 and 67–110 K are designated in Figure 10 as I, II and III, respectively. To explain the unusual dependence of the

F-centers accumulation, the following experimental results were taken into account:

• F-absorption band is more distorted in region I (insert in Figure 10) than in region II;

• from EPR data it follows that the hyperfine interaction of the F-center with the nearest interstitial fluorine [85] (or uncontrolled impurity [84]) is higher at low temperatures;

• ENDR experiments showed that the concentration of unperturbed F-centers in SrF_2 in regions I and II is small [85].

• a special cycle: irradiation, F-illumination, heating, cooling, short re-irradiation, confirmed different spatial separation of F−I pairs in regions I, II and III.

Thus, the stepwise efficiency of the formation of stable F-centers in SrF_2 is due to different spatial separation of F- and I-centers. In region I, nearby F−I-pairs are stable, and in region II, more distant F- and I-centers remain stable, etc. F-band in region I (insert of Figure 10) — a superposition of F-centers of three „types" from regions I, II and III. The considered model is also valid for BaF_2, in which the stepwise efficiency of the formation of F-centers was also recorded [84]. In CaF_2 such dependence is simpler; accordingly, the F absorption band has no structure and changes little with temperature [83]. Therefore, the F-center in CaF_2 is less perturbed than in SrF_2 and BaF_2.

The dependence of F-centers concentration on temperature in SrF_2 crystal irradiated at 20 K is represented by the curve *2* Figure 10. Since F-centers are stable (immobile) up to room temperature, the decrease in the concentration of these centers should be attributed to the mobility of hole color centers. The first decrease at 110 K lies in the region of delocalization of V_K-centers, and the second (~ 175 K) is due to the migration of H-centers and (half) V_{KA}-centers (see Figure 9) [82]. In CaF_2 and BaF_2, interaction of delocalized hole centers with F-centers and a decrease in the concentration of the latter also occurs [83,84]. Similar (stepped) curves of the dependence of the F-centers concentration on temperature were recorded in all three crystals MeF_2 irradiated with neutrons at liquid helium temperature [86].

3.3.2. High temperature region. Ionic conductivity. Crystals MeF_2 belong to the class of materials, that exhibit ionic conductivity at high temperatures (see Ch. 3 in [10]). Near the melting temperature the specific ionic conductivity (σ) in MeF_2 crystals reaches units of $\Omega^{-1} \cdot cm^{-1}$ [87]. Studies of the intrinsic conductivity of fluoride crystals at high temperatures are complicated by pyrohydrolysis, which leads to the conversion of fluorides into oxofluorides and oxides. For this reason, experiments are carried out in nitrogen atmosphere or in vacuum [88]. High-temperature ionic conductivity MeF_2 is primarily due to the hopping diffusion of anionic Frenkel α−I-pairs [5,88]. It is noted that positively charged anion vacancies in MeF_2 turn out to be more efficient in ion transport due to the lower diffusion activation energy (0.52 eV) compared to that for I-centers (0.87 eV) [89]. This situation is the opposite of that found in most other solids, where anion vacancies are less mobile than the corresponding interstices.

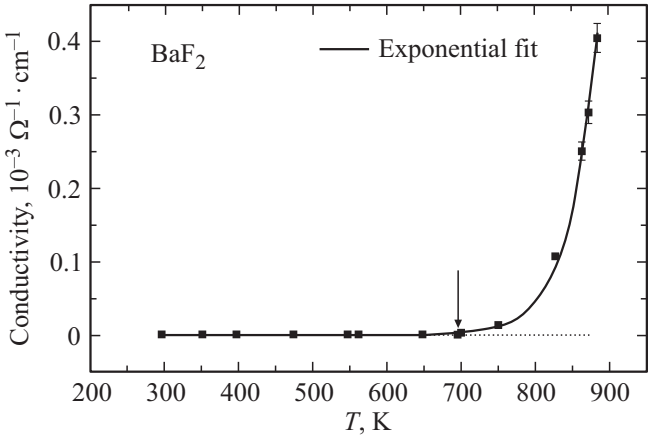

Figure 11. Temperature dependence of ionic conductivity of barium fluoride. The minimum threshold (~ 693 K) of the ionic conductivity of the crystal is noted [90].

Barium fluoride has the highest ionic conductivity among the considered MeF_2 crystals [87,88]. Figure 11 shows the ionic conductivity of barium fluoride vs. temperature [90]. At low temperatures (< 600 K) electrical conductivity is primarily due to impurity ions. The temperature increase σ is associated with increase in the crystal lattice constant BaF_2. It is shown that the minimum lattice constant required to establish a noticeable formation of anionic Frenkel defects is 6.2341 Å at ~ 580 K [90]. The minimum ionic conductivity in octahedral positions BaF_2 occurs at a threshold lattice constant of 6.2920 Å, which corresponds to temperature of 693 K and conductivity $4.64 \cdot 10^{-7}\ \Omega^{-1} \cdot cm^{-1}$ (Figure 11). At 1000 K the conductivity BaF_2 is $3.5 \cdot 10^{-3}\ \Omega^{-1} \cdot cm^{-1}$ [89]. In [91] it is shown that in the ionic conductivity BaF_2 the diffusion of anion vacancies or interstitial sites can prevail, depending on the temperature region. The effect of proton and electron irradiation on electrical conductivity CaF_2 was studied in [6], the significant role of residual impurities in changing the ionic conductivity of the crystal was discovered.

3.4. Mechanisms of defect formation

The mechanism of defect formation in ionic crystals under X-ray or VUV excitation was studied in detail using the example of AHC [45,46]. It was shown that pairs F−H are created in AHC both after optical generation of excitons (e^0), and after the creation of recombining pairs e−h, whereas α−I pairs are predominantly formed in the exciton excitation region, and in the initial region of interband transitions the efficiency of the process decreases. Conventionally, we consider „exciton" and „electron-hole" mechanisms of defect creation, although the latter is partially reduced to the first one, since holes in the valence band (within time ~ 10 ps) are autolocalized, capture

electrons from the conduction band and form excitonic states (see p. 3.1). The details of the reaction $e^0 \rightarrow F$–H remain controversial. According to [46], the formation of a pair of defects occurs at the moment of exciton transition from a one-haloid autolocalized state to two-haloid state. The defects creation at the moment of ALE transition from state with excited electronic component $(2p)$ to unexcited $(1s)$ state [92] is considered. The authors [93] believe that since the F-center is born in the ground state, and the H-center is born in the excited state, then excitation of the non-electronic component of ALE, but not of the hole component is important. It is assumed that the transition of hole $\sigma_g \rightarrow \pi_u$ (Figure 5) reduces the repulsive interaction of π-orbitals, which simplifies the separation of F- and H-centers.

As already noted, a feature of MeF_2 crystals compared to AHC is their high radiation resistance. Even when excited by ionizing particles, the point defects in MeF_2 are created with low efficiency [94]. The difference between the microprocess of defect formation in AHC and in MeF_2 is also significant. In AHC off-center ALE, which is pair of F−H-centers located along the same line, during disintegration is transformed into a pair of spatially separated F- and H-centers [45,46]. B MeF_2 off-center ALE, which also consists of a pair of nearby F−H-centers with the configuration shown in Figure 8, during disintegration it is transformed into a triplet of defects: F-, V_K- and I-centers (at low temperatures) [47.95]. It is assumed [47] that in the primary act of defect formation in MeF_2 a pair $\alpha-I$ is created, then α-center becomes F-center, capturing the electron, and the hole is autolocalized and transformed into V_K-center. This assumption is quite acceptable, taking into account that in AHC the pairs $\alpha-I$ are formed in crystals in which the distance F−H in ALE is small [45], and in MeF_2 this distance is minimal.

The exciton model of the microprocess of defect formation in MeF_2 was proposed in [72] (see the energy diagram in Figure 6). The authors estimated the energies of the $[F(1s) + H(\sigma)]$ state (~ 7 eV) and the initial state of ALE (7−8 eV), and concluded that the process of nonradiative disintegration of exciton to a pair of defects can occur spontaneously. In the paper [81] the electron-hole mechanism for the creation of F-, V_K- and I-centers in MeF_2 is proposed. It is believed that when the electron is captured from the conduction band, the F-center and the interstitial fluorine ion (I-center) are formed, and the hole is autolocalized, forming V_K-center. This becomes possible due to the low energy of formation of anionic Frenkel defects: 2.63, 2.39, 1.92 eV and high energy of electron capture per vacancy: 3.61, 3.07, 2.52 eV in CaF_2, SrF_2, BaF_2, which in turn is large due to large value of E_g in MeF_2 (in CdF_2 with lower value E_g efficiency of defect formation is low).

To create ALE in SrF_2 [79] and CaF_2 [96], electron pulses of 20 ns and energy of 2 MeV, were used, and for transient absorption spectra measurements the excimer laser or xenon lamp was used. Figure 12 shows the time-resolved absorption spectra of the crystal CaF_2 [96]. The spectrum measured in 10 μs after the end of the excitation pulse (Figure 12, *a*) is similar to the spectrum presented in Figure 7 and corresponds to ALE absorption. The electron part of ALE is responsible for the low-energy maximum, and the hole part is responsible for the high-energy maximum. The spectrum in Figure 12, c shows that under continuous irradiation at 80 K in CaF_2 stable F-centers (band with a maximum at 3.3 eV) and H-centers (band with maximum at ~ 4.0 eV) are created. From the similarity of the absorption spectra in Figure 12, *b* and *c* the conclusion was made that during additional excitation by light pulses in CaF_2 short-lived ($\sim 10\,\mu$s) F- and H- centers (no stable centers) are formed [96].

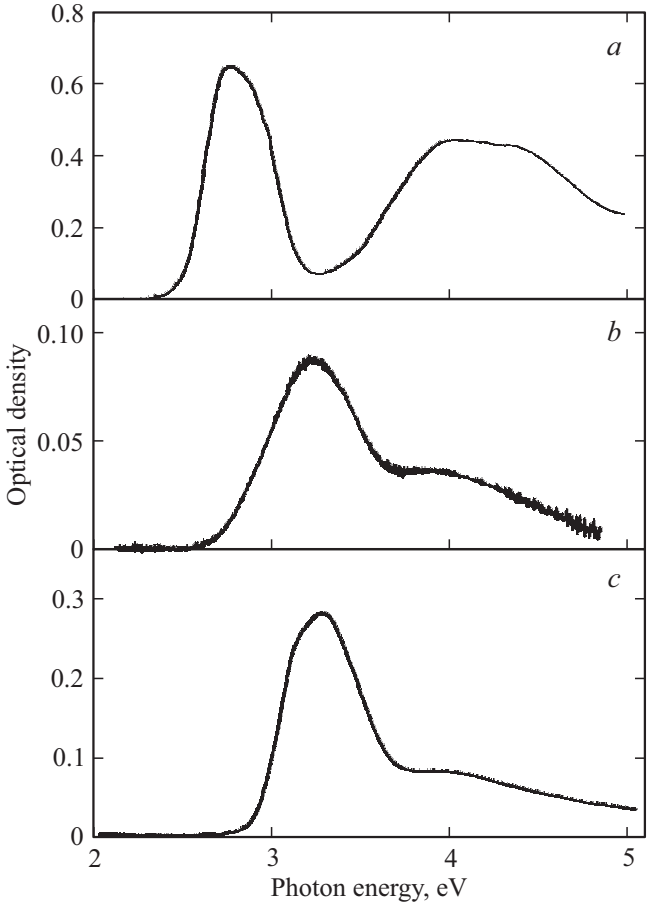

Figure 12. Time-resolved absorption spectra of crystal CaF_2 after exposure to radiation by electron pulse: *a*) 10 μs after exposure to radiation completion; *b*) difference between absorption after 0.5 and 2.0 μs; *c*) absorption spectrum during exposure to radiation by continuous electron flow ($T = 80$ K) [96].

It is shown that pulsed excitation of the hole component of ALE creates stable F-centers in CaF_2, and excitation of the electron component produces a change in the configuration of the pair F−H [79,96]. Based on this experimental fact and taking into account the low efficiency of defect formation the authors [96] concluded that additional excitation of ALE is required to create a stable defect in

CaF_2. Otherwise, the defect is generated only as a result of two successive excitations.

The idea of the electron-hole mechanism of defect formation was tested experimentally in paper [97], in which the cascade method was used to study SrF_2: pairs e−h were created by two-photon excitation with short (3.5 ps) laser pulses, and to measure absorption spectra the light pulses with 180 fs and a wavelength of 300 nm were used. This made it possible to track the behavior of the electron component of ALE, the absorption spectrum of which reached maximum for $\sim$ 500 fs and remained constant up to 43 ns. The assumption was made that in SrF_2 pairs e−h are converted in ALE during time $<$ 500 fs (in AHC this time is 5−10 ps) [97].

Using the cascade excitation method CaF_2 (two-photon laser excitation followed by transient absorption), ALE formation time was obtained to be 690 fs [98]. It was also shown that excitation of the electron part of the ALE can lead to the formation of long-lived defects. In [99] (cascade excitation method) it is shown that ALE in CaF_2 are created in two stages: fast process, which is completed within a few picoseconds, and slow process, lasting more than 20 ps. It was suggested that the precursor for the defects formation in CaF_2 is the on-center ALE (rather than the off-center proposed in [72]).

The use of transient absorption method showed that the efficiency of F-centers formation in CaF_2 increases by more than an order of magnitude in the temperature range of 300 to 500 K [100]. In general, many researchers note that the process of defect formation in MeF_2 crystals is less studied and less understood than in AHC.

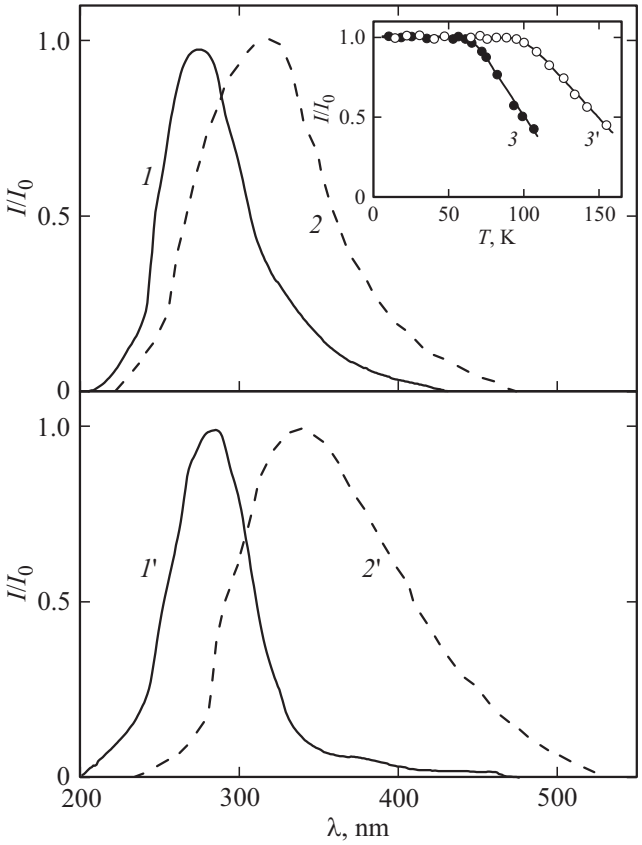

Figure 13. Spectra of X-ray luminescence CaF_2 (curves *1, 2*) and SrF_2 (*1′*, *2′*) at 80 K: long-term (*1*, *1′*) and short-term (*2*, *2′*) components [102]. Insert: temperature dependence of the intensity of the short-term ($\sim$ 10 ns) luminescence component CaF_2 (*3*) and SrF_2 (*3′*) [103].

4. Intrinsic luminescence

4.1. Emission of autolocalized excitons

4.1.1. Long-term component. The intrinsic luminescence of crystals MeF_2 was studied in detail under X-ray [47,101,102], electron [75] and VUV-excitations [23]. Figure 13 shows the spectra of X-ray luminescence CaF_2 and SrF_2 at 80 K [102] (such spectra were recorded also during electron excitation [75]). Wide ($\sim$ 1 eV) bands of luminescence are located in UV region of spectrum. The use of time-resolved mode made it possible to separate the spectra of long-term (tens of microseconds) and short-term ($\sim$ 10 ns) luminescence components (Figure 13). It was shown that triplet-singlet ($^3\Sigma_u \rightarrow {}^1\Sigma_g$) are responsible for the long-term component, and presumably singlet-singlet ($^1\Sigma_u \rightarrow {}^1\Sigma_g$) ALE transitions are responsible for the fast component [75]. In BaF_2 the intensity of the short-term luminescence component is extremely low, which did not make it possible to measure the spectrum of the corresponding luminescence.

The insert in Figure 13 shows the temperature dependence of the intensity of the short-term ($\sim$ 10 ns) luminescence component CaF_2 and SrF_2 [103]. The position of the luminescence band of this component (curves *2* and *2′*, Figure 13) is unusual, since the emission of singlet ALEs occurs from the level ($2s$) located by $\sim$ 2 eV above the triplet level ($1s$) [44.75].

In other words, the maxima of the luminescence bands of singlet ALEs shall be located at higher energies compared to those for triplet bands (which is recorded in the AHC [45]). Note that under simultaneous excitation by pulses (12 ns) of high-energy (280 keV) electrons and by photons with energy of 1.87 eV in the crystal CaF_2, UV (5.7 eV) band of fast ($\sim$ 20 ns) luminescence was recorded, the nature of which was not established [104]. The main characteristics of the intrinsic luminescence of MeF_2 crystals under X-ray excitation are given in Table 6.

At low temperatures ($T < 77$ K) constant decays of long-term components of MeF_2 luminescence that differed from each other were recorded. For example, in CaF_2 when excited by short (5 ns) electron pulses (500 keV), the decay time at $T = 10$ K consisted of three components: $\tau_1 = 83$ ns, $\tau_2 = 820\,\mu$s, $\tau_3 = 8800\,\mu$s [75]; At VUV-excitation $\tau_1 = 42$ ns, $\tau_2 = 930\,\mu$s ($T = 8$ K) [105]; at X-ray excitation $\tau_1 = 50$ ns ($T = 10$ K) [103]. The authors [106] associate this data scattering with differences in experimental conditions; however, the different origin of

Table 6. Characteristics of intrinsic luminescence of crystals under X-ray excitation: λ_m — maximum of emission band; τ_s — decay time of the long-term component; E_q — activation energy of thermal quenching; τ_f — decay time of the short-term component [75,102]

Crystal	Long-term component				Short-term component	
	λ_m, nm	τ_s, μ_s		E_q, eV	λ_m, nm	τ_f, ns
		77 K	295 K			
CaF_2	280	49	2.2	0.43	315	10
SrF_2	290	19	1.5	0.33	350	11
BaF_2	310	7.7	0.6	0.38	–	12

the crystals should also be taken into account (the presence of residual impurities in the crystals has a significant effect on the luminescence decay time [101,102]).

It is assumed that the presence of three components of the luminescence decay of MeF_2 at low temperatures is due to different ALE configurations (Figure 8). It is believed that configuration $(F,H)_{II}$ is responsible for the main component (τ_1), and the components τ_2 and τ_3 are caused by the configurations $(F,H)_I$ and $(F,H)_{III}$ [75]. This idea was developed in paper [106], in which MeF_2 crystals were irradiated at room temperature with short (170 fs) laser (5.9 eV) pulses (two-photon excitation). It is shown that after the end of the excitation pulse in the time window of 50 to 150 ns, the luminescence spectra of MeF_2 are similar to those for the long-term ALE component (curves *1* and *1′*, Figure 13). When measuring in window of 3 to 9 μs, the spectra are shifted to lower energies and broadened; the effect is especially noticeable for BaF_2, less noticeable for SrF_2 and almost not visible for CaF_2. In BaF_2, in addition to the main decay time 0.6 μs, a component with $\tau \approx 4.0\,\mu$s was recorded. Based on the data obtained, the authors [106] concluded that in addition to the configuration II of ALE, configurations I and III also take part in the radiation process, which is especially noticeable in BaF_2.

At temperatures above 77 K, a single-exponential decay in luminescence of MeF_2 was recorded, and the dependence $\tau = \tau(T)$ at electron [75] and X-ray [102] excitations corresponded to each other.

Figure 14 shows decay time of luminescence of crystals vs. temperature [102]. All three crystals show similar dependencies, which can be described by two straight lines. The activation energy of the dependence $\tau = \tau(1/T)$ in the low-temperature (80−280 K) region was 26 ± 2, 18 ± 1 and 5 ± 1 meV for CaF_2, SrF_2 and BaF_2respectively. The presence of this activation energy is associated with the existence of energy barrier for the transition of the pair (F−H) to the radiative state [89]. There are also other assumptions [102,103].

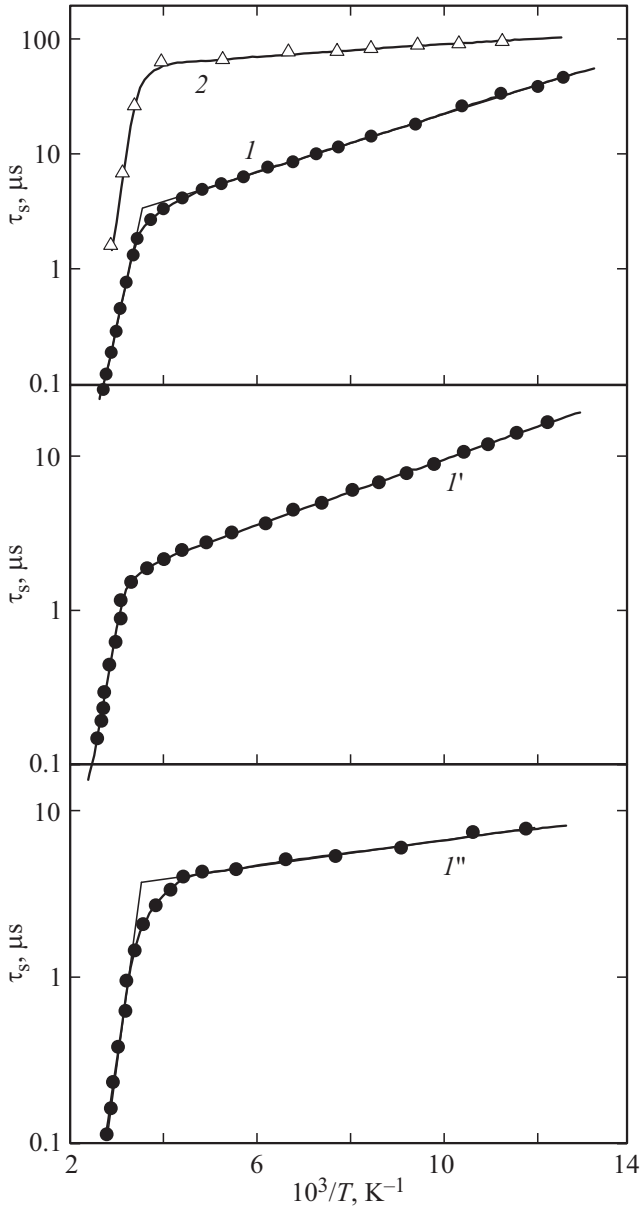

Figure 14. The decay time vs. temperature of the long-term component of luminescence of crystals CaF_2 (curve *1*), SrF_2 (*1′*) and BaF_2 (*1″*); luminescence intensity CaF_2 vs. temperature (*2*) [102].

A distinctive feature of MeF_2 crystals is high intensity of intrinsic luminescence at room temperature. In particular, in CaF_2 the light output (integrated intensity) is $\sim 50\%$ of that for the known scintillator NaI:Tl [105]. At $T > 300$ K, thermal quenching of the luminescence of MeF_2 crystals begins, this is confirmed by decrease in the radiation intensity CaF_2 (curve *2*, Figure 14). For CaF_2, SrF_2 and BaF_2, the temperature dependence of luminescence intensity was also studied in [47,107]. The activation energies of thermal quenching of luminescence (E_q), obtained from the dependences in Figure 14, are given in Table 6. The process of thermal quenching of luminescence is due to

the ALE disintegration, i. e., the diffusion of the H-center from the F-center. This is confirmed by the increase in the concentration of metastable and stable F-centers in CaF_2 at $T > 300$ K [100] (in the temperature range of 170 to 300 K F-centers in CaF_2 are absent). Consequently, the values E_q (Table 6) should be taken as the activation energy of the movement of H-centers in MeF_2. For comparison, from TSL data the activation energy of the movement of H-centers in CaF_2 — 0.46 eV [86] was obtained, which is comparable to the value given in Table 6.

Note that in alkali AHC the thermal quenching of intrinsic luminescence begins at temperatures ($T < 170$ K) slightly higher than the delocalization temperature of V_K-centers. In the case of MeF_2 the high thermal stability of the intrinsic luminescence is due to the special configuration of ALE (Figure 8).

4.1.2. Short-term component. Short-term (~ 10 ns) component of intrinsic luminescence was identified in the crystal SrF_2 [107]. The intensity of this component vs. temperature for crystals SrF_2 and CaF_2 (insert in Figure 13) was measured in [103]. Spectra of short-term component of luminescence SrF_2 and CaF_2 were obtained at electron [75] and X-ray [102] excitation.

Due to the strong overlap of intrinsic luminescence components (Figure 13), the luminescence excitation spectra were measured in time-resolved mode using synchrotron radiation [108]. Figure 15 shows the excitation spectra of short-term (~ 10 ns) and long-term (microsecond range) components of intrinsic luminescence SrF_2 ($T = 90$ K), and also, for comparison, the reflection spectrum of the crystal. The excitation spectra of the luminescence components in the region of their excitation thresholds are shown in more detailed scale for SrF_2 and CaF_2.

The spectral and kinetic parameters of the luminescence of crystals under synchrotron excitation were the same as under high-energy excitation [75,102]; in particular, in SrF_2 the emission band of the short-term component at 90 K (350 nm) was shifted to the long-wavelength region with respect to the long-term glow (300 nm).

Vata in Figure 15 show that in the studied energy ranges the luminescence excitation spectra are inverse to the reflection spectrum SrF_2. The position of the excitation thresholds for triplet component of ALE radiation is consistent with the onsert of fundamental absorption of crystals and the creation of excitons with the lowest energy in them [23]. The energy difference between the excitation thresholds of the slow and fast ALE components in SrF_2 and CaF_2 was 0.5−0.6 eV. This ratio of excitation thresholds is typical for a number of AHCs, since singlet-singlet transitions in them occur from high orbital states [45,72]. Thus, according to the excitation spectra and the luminescence decay time, the short-term component CaF_2 and SrF_2 corresponds to the characteristics of singlet ALEs, but according to the luminescence spectra it does not correspond. Note that the time-resolved luminescence spectra and luminescence excitation spectra of MeF_2 were measured at low temperature (17 K) [l09], but this did not

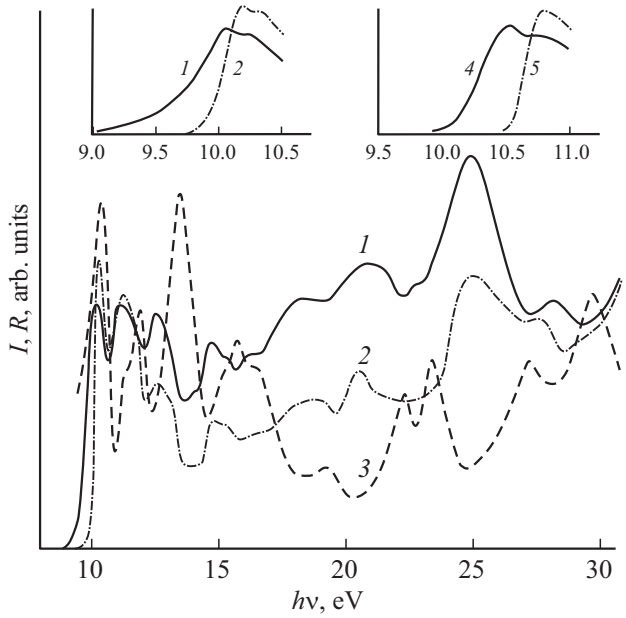

Figure 15. Excitation spectra of long-term (curves *1, 4*) and short-term (*2, 5*) components of ALE luminescence SrF_2 (*1, 2*) and CaF_2 (*4, 5*) at 90 K. Reflection spectrum SrF_2 (*3*) at 295 K [108].

contribute noticeably to understanding the mechanism of short-term emission of ALE.

Thermal quenching of the short-term luminescence component (insert in Figure 13) begins at temperatures slightly lower than the delocalization temperatures of V_K-centers in CaF_2 and SrF_2 (Table 5). Based on this fact and a number of other considerations, the authors [45,72] suggested that on-center ALEs, i. e., $e^0(V_K + e)$, are responsible for the short-term component of luminescence. Note that in CaF_2 the distance between fluorine atoms in V_K-center [10] and in H-center [69] is 1.85 and 1.90 Å respectively. The smaller this distance is, the stronger the axial relaxation of the molecular ion F_2^- is, and the greater the Stokes shift (the difference in the energies of free and autolocalized excitons) is. Then the process of ALE radiation can be represented as follows. In the primary act V_K-center captures the electron, forming exciton $e^0(V_K + e)$, which emits during ~ 10 ns ($^1\Sigma_u \rightarrow {}^1\Sigma_g$-ALE transitions). Then the state $e^0(V_K + e)$ is converted into exciton e^0(F,H), which is a source of triplet luminescence ($^3\Sigma_u \rightarrow {}^1\Sigma_g$-ALE transitions). In this model, the overlap of the emission spectra of singlet and triplet excitons (Figure 13) is due to the fact that the hole components of ALE are in different states: in the first case in the form of V_K-center, in the second case — H-center.

When excited by short (600 fs) laser pulses in SrF_2 and CaF_2, a short-term (~ 0.5 ns) luminescence component was recorded at room temperature [l10]. The authors concluded that this emission is associated with the rapid decay of excitons in F−H-pairs, or with the emission of singlet excitons from hot states.

4.2. Core-valence transitions (BaF_2)

Core-valence transitions(CVT) in barium fluoride (other names for this fast luminescence — cross-luminescence and Auger-free luminescence) will be considered briefly, since their characteristics are described in detail in a recent paper [111]. Radiative CVTs become possible if the energy gap (ΔE_{cv}) between the upper core and valence bands is less than the band gap (E_g) of the crystal: $\Delta E_{cv} < E_g$. The fulfillment of this condition depends on the position of the upper core zone. In contrast to CaF_2, where the gap between the upper core band and the conduction band (ΔE_{cc}) is ~ 25 eV (Figure 3), in BaF_2 $\Delta E_{cc} \approx 18$ eV, which leads to the fulfillment of the condition $\Delta E_{cv} < E_g$. Radiative CVTs were first discovered in the study of X-ray luminescence BaF_2 (see details in [12,111]). In contrast to „conventional" luminescence, which occurs within the band gap, radiative CVTs occur between the upper core and valence bands of the crystal. Currently, there are dozens of compounds in which this new type of luminescence was identified.

Radiative CVTs are characterized by short decay times ($\tau < 3$ ns) and high temperature stability, which makes it possible to use crystals with this type of luminescence as ultrafast scintillators. One of the best ultrafast scintillators BaF_2 has decay time of 0.8 ns. Studies and search for CVTs that are interesting from scientific and applied point of view are actively developing [112,113].

5. Conclusion

Analysis of experimental and theoretical data showed that CaF_2, SrF_2 and BaF_2 represent a class of crystals with special physical properties determined first of all by the crystalline structure of objects. CaF_2 has the best characteristics among the fluorides under study: high radiation resistance, transparency in the VUV region of the spectrum, uniformity of the refraction index, lack of hygroscopicity. The use of two-photon laser spectroscopy made it possible to identify exciton peaks at the fundamental absorption edge CaF_2 and its analogues [38]. Recent achievements also include method of CaF_2 growing in argon flow to obtain high-quality crystals whose optical properties meet the requirements of microphotolithography [14,37].

In MeF_2 stable point defects are effectively formed under the influence of ionizing radiation only at low ($T \leq 77$ K) temperatures.

Many characteristics of point defects in MeF_2 differ from those in AHC and other ionic crystals. The primary radiation defects in MeF_2 are F, V_K- and I-centers. When heated V_K-centers diffuse, interact with I-centers and form H-centers. SrF_2 and BaF_2 are characterized by stepwise efficiency of formation of stable F-centers, due to different spatial separation of F-and I-centers. The autolocalized exciton in MeF_2 consists of a pair of nearby F−H-centers with the configuration shown in Figure 8. The main levels of hole V_K- and H-centers are located in the band gap ranging from 1.0 to 2.0 eV above the valence band. For BaF_2 we were able to determine the position of the main level of I-center: ~ 0.6 eV from the top of the valence band.

The use of transient absorption and cascade excitation methods made it possible to significantly advance the understanding of defect formation processes in the crystals under study. However, there is no consensus among researchers about the initial configuration from which point defects are formed in crystals with fluorite structure. Residual impurities may participate in the process of defect formation; for this reason, the experimental data obtained on the optical properties of color centers in crystals do not always correspond to each other.

The high intensity of intrinsic (exciton) luminescence of MeF_2 at room temperature is due to the special configuration of autolocalized excitons in the form of nearby F−H-pairs. The issue of mechanism of short-term luminescence of MeF_2 remains debatable. To solve this problem, it is necessary to carry out experiment at low temperatures, carried out in [110] at room temperature (at which this luminescence is practically extinguished).

Acknowledgments

The author expresses gratitude to V.M. Khanin and I.D. Venevtsev for their assistance in carrying out this study and useful discussions of the material.

Conflict of interest

The author declares that he has no conflict of interest.

References

[1] P.P. Feofilov. Acta Phys. Polon. **26**, *3–4*, 331 (1964).
[2] AA Kaplyansky. Optika i spektroskopiya **16**, *2*, 602 (1964). (in Russian).
[3] V.V. Osiko. FTT **7**, *5*, 1294 (1965). (in Russian)
[4] A.I. Ryskin, A.E. Angervaks, A.V. Veniaminov. In: Holographic Materials. Optical Systems. Intech (2017). Ch. 18. P. 405−433.
[5] B.P. Sobolev. Crystallogr. Reps **65**, *5*, 678 (2020).
[6] V.M. Lisitsyn. Izv. Tomsk. politekh. instituta **247**, 56 (1977). (in Russian).
[7] H.B. Starostin, M.P. Shepilov. FTT **17**, *3*, 822 (1975). (in Russian).
[8] V.M. Reuterov, Z.N. Korneva. Optika i spektroskopiya **21**, *5*, 583 (1966). (in Russian).
[9] E. Radzhabov. J. Phys: Condens. Matter **6**, *45*, 9807 (1994).
[10] Crystals with Fluorite Structure / Ed. W. Hayes. Oxford University Press, London (1974). 448 p.
[11] Yu.M. Alexandrov, V.N. Makhov, P.A. Rodny, T.I. Syreyshchikova, M.N. Yakimenko. FTT **26**, *9*, 2865 (1984). (in Russian).
[12] P.A. Rodny. FTT **34**, *7*, 1975 (1992). (in Russian).
[13] C. Gorling, U. Leinhos, K.R. Mann. Opt. Commun. **249**, *1*, 319 (2005).
[14] J.T. Mouhovski. Prog. Cryst. Growth Charact. Mater. **53**, *2*, 79 (2007).

[15] Y. Shimizu, M. Minowa, W. Suganuma, Y. Inoue. Phys. Lett. B **633**, *2–3*, 195 (2006).
[16] M. Verstraete, X. Gonze. Phys. Rev. B **68**, *19*, 195123 (2003).
[17] V.A. Chernyshev, V.S. Ryumshin, P.A. Agzamova. Phys. Solid State **61**, *1*, 11 (2019).
[18] Crystal Structures / Ed. R.W.G. Wyckoff. Interscience. John Wiley, N.Y. (1963). 467 p.
[19] R. Saravanan, S. Israel. Physica B **352**, *1–4*, 220 (2004).
[20] G.W. Rubloff. Phys. Rev. B **5**, *2*, 662 (1972).
[21] J. Frandon, B. Lahaye, F. Pradal. Phys. Status Solidi B **53**, *2*, 565 (1972).
[22] J. Barth, R.L. Johnson, M. Cardona, D. Fuchs, A.M. Bradshaw. Phys. Rev. B **41**, *5*, 3291(R) (1990).
[23] A.J. Bourdillon, J.H. Beaumont. J. Phys. C **9**, *17*, L479 (1976).
[24] V.V. Sobolev, A.I. Kalugin. Semiconductors **36**, *2*, 148 (2002).
[25] E.R. Il'mas, G.G. Lydya, Ch.B. Lushchik. Optika i spektroskopiya **18**, *3*, 453 (1965). (in Russian).
[26] M. Letz, A. Gottwald, M. Richter, L. Parthier. Phys. Rev. B **79**, *19*, 195112 (2009).
[27] P.J. Singh, A. Gupta, A.K. Das, V. Kumar, A. Shastri, B.N. Rajasekhar. AIP Conf. Proc. **2265**, *2*, 030426 (2020).
[28] N.V. Starostin, M.P. Shepilov, A.B. Alekseev. Phys. Status Solidi B **103**, *2*, 717 (1981).
[29] M. Catti, A. Pavese, V.R. Saunders. J. Phys. C **3**, *23*, 4151 (1991).
[30] H. Shi, R.I. Eglitis, G. Borstel. Phys. Status Solidi B **242**, *10*, 2041 (2005).
[31] E. Cadelano, G. Cappellini. Eur. Phys. J. B **81**, *1*, 115 (2011).
[32] B. Bohara, B L. Franklin, Y. Malazovsky, D. Bagayoko. Proc. Louisiana EPSCoR RII LA-SiGMA, 1 (2015).
[33] F. Matusalem, M. Marques, L.K. Teles, A. Filippetti, G. Cappellini. J. Phys.: Condens. Matter **30**, *36*, 365501 (2018).
[34] R.T. Poole, J. Szajman, R.C.G. Leckey, J.G. Jenkin, J. Liesegang. Phys. Rev. B **12**, *12*, 5872 (1975).
[35] M. Huisinga, M. Reichling, E. Matthias. Phys. Rev. B **55**, *12*, 7600 (1997).
[36] T. Tsujibayashi, K. Toyoda, S. Sakuragi, M. Kamada, M. Itoh. Appl. Phys. Lett. **80**, *16*, 2883 (2002).
[37] J.H. Burnett, R. Gupta, U. Griesmann. Appl. Optics **41**, *13*, 2508 (2002).
[38] E.I. Rashba. Bull. A.S. USSR. Phys. Ser. **40**, *9*, 20 (1976).
[39] I.G. Lang. JETP **45**, *6*, 1130 (1977).
[40] T.G. Castner, W. Känzig. J. Phys. Chem. Solids **3**, *3–4*, 178 (1957).
[41] R. Gazzinelli, R.L. Mieher. Phys. Rev. **175**, *2*, 395 (1968).
[42] V.E. Puchin, A.L. Shluger, K. Tanimura, N. Itoh. Phys. Rev. B **47**, *11*, 6226 (1993).
[43] K. Kan'no, T. Matsumoto, Y. Kayanuma. Pure. Appl. Chem. **69**, *6*, 1227 (1997).
[44] K.S. Song, R.T. Williams. Self-Trapped Excitons. Springer-Verlag, N.Y. (1993). Ch. 4.
[45] C.B. Lushchik, I.K. Vitol, M.A. Élango. Phys. — Usp. **20**, *6*, 489 (1977).
[46] C. Lushchik, A. Lushchik. Phys. Solid State **60**, *8*, 1487 (2018).
[47] J.H. Beaumont, W. Hayes, D.L. Kirk, G.P. Summers. Proc. R. Soc. Lond. A **315**, *1520*, 69 (1970).
[48] K.-D. Li, H.Y. Xiao, L.M. Wang. Nucl. Instr. Meth. Phys. Res. B **266**, *12–13*, 2698 (2008).
[49] Y. Ma, M. Rohlfing. Phys. Rev. B **77**, *11*, 115118 (2008).
[50] C.H. Seager. Phys. Rev. B **3**, *10*, 3479 (1971).
[51] N.N. Ershov, N.G. Zakharov, V.M. Reuterov, P.A. Rodny. Optika i spektroskopiya **52**, *2*, 372 (1982). (in Russian).
[52] A.I. Nepomnyashchikh, E.A. Radzhabov, A.V. Egranov, V.F. Ivashechkin, A.S. Istomin. Rad. Eff. Defects. Solids: Incorporating Plasma Sci. Plasma Technol. **157**, *6–12*, 715 (2002).
[53] T. Eshita, K. Tanimura, N. Itoh. Nucl. Instrum. Meth. Phys. Res. B **1**, *2–3*, 452 (1984).
[54] S. Stepanov, E. Chinkov, A. Shrayber, V. Shtan'ko. Rad. Phys. Chem. **191**, 109889 (2022).
[55] W. Chen, P. Song, Y. Dong, Y. Zhang, W. Hua. Chin. Sci. Bull. **58**, *11*, 1321 (2013).
[56] D.W. Cooke, B.L. Bennett. J. Nucl. Mater. **321**, *2–3*, 158 (2003).
[57] R. Rauch, G. Schwotzer. Phys. Status Solidi A **74**, *1*, 123 (1982).
[58] B.G. Ravi, S. Ramasamy. Int. J. Mod. Phys. B **06**, *17*, 2809 (1992).
[59] V.A. Arkhangelskaya, P.P. Feofilov. Kvantovaya elektron. **7**, *6*, 1141 (1980). (in Russian).
[60] H. Shi, L. Chang, R. Jia, R.I. Eglitis. J. Phys. Chem. C **116**, *7*, 4832 (2012).
[61] L.P. Cramer, S.C. Langford, J.T. Dickinson. J. Appl. Phys. **99**, *5*, 054305 (2006).
[62] E.A. Kotomin, A.I. Popov. In: Radiation Effects in Solids (NATO Sci. Ser. II: Mathematics, Physics and Chemistry / Eds K.E. Sickaufus, E.A. Kotomin, B.P. Uberuaga) **235**, 153 (2007). Ch. 7.
[63] M.N. Kabler. In: Point Defects in Solids / Eds J.H. Crawford Jr, LM. Slifkin. Plenum Press, N.Y. (1972). P. 327−380.
[64] V.A. Arkhangelskaya, L.A. Alekseeva. Optika i spektroskopiya **21**, *I*, 93 (1966). (in Russian).
[65] M.J. Norgett, A.M. Stoneham. J. Phys. C **6**, *2*, 229 (1973).
[66] N. Chuklina, A. Mysovsky. Rad. Measur. **128**, 106135 (2019).
[67] W. Hayes, R.F. Lambourn, J.P. Stott. J. Phys. C **7**, *14*, 2429 (1974).
[68] V.P. Zhukov, V.M. Zainullina. Phys. Sold State **40**, *11*, 1827 (1998).
[69] S. Parker, K.S. Song, C.R.A. Catlow, A.M. Stoneham. J. Phys. C **14**, *28*, 4009 (1981).
[70] H. Shi, R. Jia, R.I. Eglitis. Comput. Mater Sci. **89**, 247 (2014).
[71] R. Jia, H. Shi, G. Borstel. J. Phys. : Condens. Matter **22**, *5*, 055501 (2010).
[72] M.N. Kabler, R T. Williams. Phys. Rev. B **18**, *4*, 1948 (1978).
[73] P.J. Call, W. Hayes, M.N. Kabler. J. Phys.: Solid State Phys. **8**, *4*, L60 (1975).
[74] N.G. Romanov, V.A. Vetrov, P.G. Baranov. JETP Lett. **37**, *7*, 386 (1983).
[75] R.T. Williams, M.N. Kabler, W. Hayes, J.P. Stott. Phys. Rev. B **14**, *2*, 725 (1976).
[76] M. Adair, C.H. Leung, K.S. Song. J. Phys. C **18**, *28*, L909 (1985).
[77] K.S. Song, C.H. Leung, J.M. Spaeth. J. Phys.: Condens. Matter **2**, *30*, 6373 (1990).
[78] C.H. Leung, C.G. Zhang, K.S. Song. J. Phys.: Condens. Matter. **4**, *6*, 1489 (1992).

[79] T. Eshita, K. Tanimura, N. Itoh. Phys. Status Solidi B **l22**, *2*, 489 (1984)
[80] A. Mysovsky, E. Radzhabov. IEEE Trans. Nucl. Sci. **57**, *3*, 1200 (2010).
[81] C.R.A. Catlow. J. Phys. C **12**, *6*, 969 (1979).
[82] M.J. Norgett, A.M. Stoneham. J. Phys. C **6**, *2*, 238 (1973).
[83] W. Hayes, R.F. Lambourn. Phys. Status Solidi B **57**, *2*, 693 (1973).
[84] P.J. Call, W. Hayes, J.P. Stott, A.E. Hughes. J. Phys. C **7**, *14*, 2417 (1974).
[85] W. Hayes, R.F. Lambourn. J. Phys. C **6**, *1*, 11 (1973).
[86] K. Atobe. J. Chem. Phys. **71**, *6*, 2588 (1979).
[87] B.M. Voronin, S.V. Volkov. J. Phys. Chem. Solids **62**, *7*, 1349 (2001).
[88] N.I. Sorokin, B.P. Sobolev. Phys. Solid State **60**, *12*, 2450 (2018).
[89] P.W.M. Jacobs, S.H. Ong. J. Physique C7 **37**, *12*, 331 (1976).
[90] T.P. Jili, E. Sideras-Haddad, D. Wamwangi, D. Billing, C.L. Ndlangamandla, M. Khulu. South African Instit. Phys. Proc. 64th Annual Conf. 82 (2019).
[91] V.M. Carr, A.V. Chadwick, D.R. Figueroa. J. Physique C7 **37**, *12*, 337 (1976).
[92] Y. Toyozawa. J. Phys. Soc. Jpn. **44**, *2*, 482 (1978).
[93] N. Itoh, A.M. Stoneham, A.H. Harker. J. Phys. C **10**, *21*, 4197 (1977).
[94] N. Itoh, K. Tanimura. Rad. Effects. Defects. Solids **98**, *1–4*, 269 (1986).
[95] M. Watanabe, J. Azuma, S. Asaka, T. Tsujibayashi, O. Arimoto, S. Nakanishi, H. Itoh, M. Kamada. Phys. Status Solidi B **250**, *2*, 396 (2013).
[96] K. Tanimura, T. Katoh, N. Itoh. Phys. Rev. B **40**, *2*, 1282 (1989).
[97] E.D. Thoma, H.M. Yochum, R.T. Williams. Phys. Rev. B **56**, *13*, 8001 (1997).
[98] R. Lindner, M. Reichling, R.T. Williams, E. Matthias. J. Phys.: Condens. Matter **13**, *10*, 2339 (2001).
[99] K. Tanimura. Phys. Rev. B **63**, *18*, 184303 (2001).
[100] S.I. Kachan, E.E. Obukhova, S.A. Stepanov, E.P. Chinkov, V.F. Shtan'ko. Chem. Met. Alloys **4**, 26 (2011).
[101] Yu.B. Vladimirsky, G.M. Zakharov, T.I. Nikitinskaya, V.M. Reuterov, P.A. Rodny. Optika i spektroskopiya **32**, *4*, 756 (1972). (in Russian).
[102] N.N. Ershov, N.G. Zakharov, P.A. Rodny. Optika i spektroskopiya **53**, *1*, 89 (1982). (in Russian).
[103] A.V. Agafonov, P.A. Rodny. FTT **25**, *2*, 289 (1983). (in Russian).
[104] V. Shtan'ko, E. Chinkov, A. Shrayber, S. Stepanov. Rad. Phys. Chem. **168**, 108619 (2020).
[105] V.B. Mikhailik, H. Kraus, J. Imber, D. Wahl. Nucl. Instr. Meth. Phys. Res. A **566**, *2*, 522 (2006).
[106] R. Lindner, R.T. Williams, M. Reichling. Phys. Rev. B **63**, *7*, 075110 (2001).
[107] T.I. Nikitinskaya, P.A. Rodny, S.B. Mikhrin. Optika i spektroskopiya **39**, *3*, 411 (1975). (in Russian).
[108] Yu.M. Alexandrov, V.N. Makhov, P.A. Rodny, T.I. Syreyshchikova, M.N. Yakimenko. FTT **28**, *9*, 2853 (1986). (in Russian).
[109] J. Becker, M. Kirm, V.N. Kolobanov, V.N. Makhov, V.V. Mikhailin, A.N. Vasil'ev, G. Zimmerer. Electrochem. Soc. Proc. **98**, *25*, 415 (1998).
[110] N. Fedorov, A. Belsky, E. Constant, D. Descamps, P. Martin, A.N. Vasil'ev. J. Lumin. **129**, *12*, 1813 (2009).
[111] V. Khanin, I. Venevtsev, P. Rodnyi. Opt. Mater. **136**, 113399 (2023).
[112] M. Cadatal-Raduban, A. Yoshikawa, L.V. Mui, M.H. Pham, T. Shimizu, N. Sarukura, T. Togashi, K. Yamanoi. Jpn. J. Appl. Phys. **59**, *5*, 052005 (2020).
[113] G. Konstantinou, R. Latella, L. Moliner, L. Zhang, J.M. Benlloch, A.J. Gonzalez, P. Lecoq. Phys. Med. Biol. **68**, *2*, 025018 (2023).

Translated by I.Mazurov